Additive Manufacturing 63 (2023) 103417

Contents lists available at ScienceDirect

Additive Manufacturing

journal homepage: www.elsevier.com/locate/addma

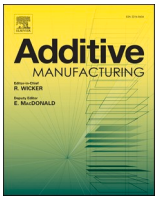

Assessment of the benefits of 3D printing of advanced thermosetting composites using process simulation and numerical optimisation

Giacomo Struzziero [a,*], Michel Barbezat [a], Alexandros Antonios Skordos [b]

[a] Laboratory for Mechanical Systems Engineering, Swiss Federal Laboratories for Materials Science and Technology (Empa), Überlandstrasse 129, 8600 Dübendorf, Switzerland
[b] School of Aerospace, Transport and Manufacturing, Cranfield University, Bedford MK43 0AL, UK

ARTICLE INFO

Keywords:
Thermosetting resin
3D printing
Continuous fibres
Thick composites

ABSTRACT

3D printing of continuous fibre reinforced thermosetting matrix composites is set to revolutionise composite manufacturing practice. The potential of curing additively is anticipated to bring significant improvement in terms of increasing process speed, producing geometries that are inaccessible with current processing routes and eliminating detrimental exothermic effects during the process. This study presents a comparison between the curing stage of the 3D printing and standard batch processing for carbon fibre/epoxy components of varying thickness and size. An optimisation methodology links simulation of the cure using Finite Element solver Abaqus with a Genetic Algorithm capable of dealing with multi-objective problems. Optimal cure cycles to minimise both process time and temperature overshoot in 3D printing and batch processing are identified and the optimal trade-offs compared. The results highlight that temperature overshoot reduction up to 85 % is possible and that the intrinsic additive nature of the 3D printing allows eliminating the dependence of temperature overshoot on thicknesses and producing components with thicknesses that are very difficult to manufacture conventionally. A simplified procedure for the estimation of 3D printing process duration is proposed based on the results of finite element simulation. This is used for exploration of the limits of the process with respect to part size and for a generic comparison of process applicability against batch processing. The analysis shows that 3D printing is highly advantageous for small components, is efficient for mid-size components and can – on the basis of its scalability – offer a feasible route for producing large and very large components.

1. Introduction

Continuous fibre thermosetting composites have several advantages compared to standard materials such as high strength to weight ratio and anisotropic nature allowing weight reduction associated with environmental benefits and structural efficiency as well as additional design flexibility and opportunities for tailoring component design. Nevertheless, the manufacturing of composites does not meet the tight sustainability requirements currently sought. Industry relies on conservative cure cycles with the drawback of large energy consumption which increases cost and CO_2 emissions. The problem becomes even more challenging for thick thermosetting composite components. Due to the low thermal conductivity in the through thickness direction and the strong non-linearity of the exothermic reaction involved, it is not trivial to set up cure cycles capable of curing thick parts that can meet stringent quality requirements. Often defects such as under-cured regions and high overshooting temperatures are the cause of part rejection which is problematic in terms of both sustainability and cost. In light of current CO_2 emission targets, the industry needs to improve the way composites are manufactured to reduce energy consumption and to reach a first-time right approach towards zero environmental impact.

In the last two decades research has focussed on improving manufacturing outcomes by adopting optimisation methodologies in combination with accurate simulation of the curing process [1]. Significant improvements have been obtained in terms of process time (i.e. cost and energy consumption) [2–4] and cure-induced defects minimisation (i.e. residual stresses) [5,6]. Furthermore, understanding the interconnected nature of the objectives at play, latest trends suggest the use of multi-objective methodology for the design stage. The implementation of multi-objective methodologies has led to comprehensive understanding of the complexity of the landscape of the process design problem and to efficient and effective ways to achieve first-time right

* Corresponding author.
E-mail address: giacomo.struzziero@empa.ch (G. Struzziero).

https://doi.org/10.1016/j.addma.2023.103417
Received 7 October 2022; Received in revised form 16 December 2022; Accepted 13 January 2023
Available online 14 January 2023

manufacturing. The design solution obtained in a multi-objective problem is in the form of a Pareto front, which represents the trade-offs between relevant objectives [7,8]. Examination of the Pareto front demonstrates the non-linear character of the problem, which involves increasing complexity as the thickness of the manufactured component increases [8].

3D printing of continuous fibre composites is envisioned as a process that allows the composite manufacturing industry to leap forwards to meet sustainability targets. The technology is not mature currently; however, some works have demonstrated its potential application to thermoplastic [9–13] and thermosetting [14–17] matrix composites. 3D printed thermosetting composites have been found to have better mechanical properties than similar 3D printed thermoplastic composites [14]. Nevertheless, the flexural strength achieved is 50 % lower compared to standard manufacturing routes (860 MPa versus 1703 MPa), tensile strength is 68 % lower (1476 MPa versus 2171 MPa) and interlaminar shear strength is 46 % lower (49 MPa versus 107 MPa) [18]. The Layer by Layer (LbL) curing process has been proposed as an additive composite manufacturing route allowing to move away from the highly non-linear dependence of the curing process on thickness [19]. The new concept has its foundation on the finding that composite interfacial properties are retained as long as pre-cured sublaminates are not beyond the gelation point at the moment of the deposition and consolidation of the subsequent layer [19]. The concept of LbL can be extended to 3D printing of continuous fibre thermoset composites. The modelling and simulation of the phenomena involved in 3D printing process of thermosetting composite materials have not been addressed yet. The curing cycle can be optimised to minimise residual stress and optimise performance. Mechanical properties evolve as a function of the degree of cure and temperature. Therefore, the coupling between the reaction kinetics and the mechanical properties evolution of the resin needs to be addressed to optimise performance [20]. Furthermore, simulation can provide the impetus for further development of 3D printing processing through exploring its benefits in the context of manufacturing efficiency.

The current paper addresses the heat transfer simulation and optimisation of the cure in a 3D printing process using continuous carbon fibres. The optimisation methodology, which is applied to a material system appropriate for Liquid Composite Moulding, includes the cure cycle and printing speed as optimisation parameters with the objective to minimise process time and temperature overshoot. The Pareto fronts obtained from the optimisation are compared with those from the solution obtained in optimisation of standard manufacturing routes to establish the levels of potential benefits of the 3D printing process. Based on the results of finite element modelling a simplified and generic framework is put forward for the approximation of 3D printing process duration. This is utilised for an exploratory investigation of the capability of 3D printing to produce continuous fibre/thermosetting matrix structures across different component scales for both Liquid Moulding Composite and prepreg material systems.

2. Simulation of the cure process

The thermo-chemical phenomena governing the curing process of thermosetting composites have been modelled using the FE solver Abaqus® [21]. The materials of this study are G1157 carbon fibres [22]. RTM6 epoxy system [23] and the HexPly® M21 prepreg epoxy system [24]. The evolution of the cure process has been studied for two scenarios: i) standard batch curing manufacturing in an oven and; ii) 3D printing. In batch composite manufacturing routes, such as autoclaving and Liquid Composite Moulding (LCM), curing happens simultaneously for the whole component once the previous manufacturing steps (consolidation, filling) have been completed.

A total of four configurations have been used and summarised in Table 1, which reports the different dimensions of the parts and the process they have been used for alongside the material system adopted in the simulation/optimisation. The composite parts comprise UD layers or tows depending on the process scenario examined. The tow thickness considered is 2 mm [14]. Three dimensional isoparametric 8-node brick composite elements suitable for heat transfer analysis have been utilised. In 3D printing simulation, the newly generated elements are assumed to form a perfect contact with the already deposited elements; this assumption makes heat transfer more effective than in reality. The total numbers of elements was 6,000, 9,000 and 12,000 elements for Case I, II and III respectively and 22,500 elements for Case IV. The dimensions were chosen to limit computational time while at the same time resulting in expected three-dimensional heat transfer behaviour in the AM simulation. The solution of standard batch process can be approximated as an 1D heat transfer problem. This is an assumption often made in the simulation of composite batch processes, especially in the context of optimisation where computational efficiency is necessary, due to the predominantly 1D character of the geometries involved as evidenced by experimental validation [8,25]; therefore, the corresponding model was constructed using one element in the in-plane dimensions and 27, 40 and 53 elements across the thickness for Case I, II and III respectively. The number of elements is chosen as a compromise between accuracy in temperature overshoot prediction and computational time as the model is used iteratively in optimisation. An adaptive time step with a threshold in temperature change of 2 °C has been used for the standard batch process simulation. In the simulation of the AM process of Case I, II, III, a fixed time step of 30 s has been used, whilst for Case IV a 120 s fixed time step was adopted. A time step of 120 s allows speeding up the simulation with negligible effects on temperature (average error about 0.4 °C) and degree of cure prediction (average error about 0.05), which corresponds to a maximum inaccuracy in process time of about ± 60 s. The non-linear material properties and behaviour including cure kinetics, specific heat and thermal conductivity have been assigned using the UMATHT user subroutine [21]. Prescribed temperature boundary conditions were applied through the DISP user subroutine following the cure cycle, whilst a convection boundary condition was applied using the FILM user subroutine [21]. Standard process is assumed to occur within an oven and therefore the convection coefficient is selected equal to 50 $W/m^2/°C$ [26], the 3D printing is assumed to use forced convection through a heating gun, therefore a convection coefficient of 350 $W/m^2/°C$ has been chosen, whilst the ambient temperature follows the cure cycle. The value of 350 $W/m^2°C$ has been chosen to accelerate surface heating of deposited tows. In a physical implementation, this is achievable by using impinging air jets (i.e. heat guns) [27–30]. In the 3D printing case, a moving convection boundary condition has been applied to the top surfaces at any instant and at the sides, the boundary condition is progressively deactivated on the surfaces where elements have been deposited; whilst in the standard batch process insulation is applied at the sides of the component making the heat transfer problem one dimensional. The volume fibre fraction is around 57 % for RTM6 and 60 % for the HexPly® M21 prepreg case. The geometries used for the two manufacturing cases are the same and the

Table 1
Summary of configurations used for simulation.

	Dimensions			Simulation/Optimisation		
	Length (mm)	Width (mm)	Thickness (mm)	3D printing (Liquid-RTM6)	3D printing (Prepreg-M21)	Standard (LCM-RTM6)
Case I	40	20	20	✓	✓	✓
Case II	40	20	30	✓	✓	✓
Case III	40	20	40	✓	✓	✓
Case IV	150	20	20	✓		

boundary conditions reflect the differences between the two processing strategies. The constitutive material models are represented by a set of equations expressing dependence on both temperature and degree of cure; these include cure kinetics, specific heat of the resin, fibres and composite, glass transition temperature evolution, and thermal conductivity of the resin, fibre and composite. A schematic representation of the boundary condition set applied to the two scenarios is depicted in Fig. 1. In Fig. 1, the z direction corresponds to the thickness of the component. In the AM process, the longitudinal direction of fibres is along the printing direction. The tool is also shown in the schematic for clarity of representation. However, in the model the tool is replaced by the presence of the prescribed temperature boundary condition. In the case of the batch process, the prescribed temperature and ambient temperature follow a typical cure profile comprising two isothermal segments (dwells). For 3D printing, the profile comprises a single isothermal segment. Fig. 2 illustrates the cure profiles adopted.

Initial conditions were applied using user subroutine USDVINI [21], with initial degree of cure equal to 0.02 and temperature equal to the deposition temperature (i.e. temperature at the printing head) for the 3D printing scenario. The tow is represented by three elements across the thickness and a single element across the width, whilst the initial temperature at the moment of deposition is assumed uniform. The initial temperature for the batch process was 120 °C based on the standard tool temperature during infusion of RTM6 resin [23]. Furthermore, the user subroutine UEPACTIVATIONVOL [21] has been used to progressively activate elements as they are deposited in the 3D printing model. A conventional batch curing process for RTM6 dictates that the resin is infused at 120 °C (T_0). Once the infusion step is concluded, curing starts. The material can be heated from 120 °C to 180 °C at 1 °C/min and the dwell temperature kept for 120 min [23] or heated up to 160 °C at 1 °C/min, 45 min dwell and heated up to 180 °C and kept 120 min at this temperature [31]. For the 3D printing scenario, the material is deposited at 150 °C on a hot tool heated at 180 °C.

The heat transfer problem is as follows:

$$\rho_c c_p \frac{\partial T}{\partial t} = \nabla \bullet (\mathbf{K}\nabla T) + \rho_r v_r H_{tot} \frac{d\alpha}{dt} \tag{1}$$

Here ρ_c, c_p are the density and specific heat of the composite, **K** is the thermal conductivity tensor, ρ_r the resin density, H_{tot} the total heat flow and α the degree of cure.

The cure kinetics, glass transition temperature development and thermal properties of the RTM6 epoxy system have been extensively studied and a full set of the corresponding constitutive models has been established [31–33] including experimental validation of the accuracy of heat transfer model of the cure [34]. The HexPly® M21 prepreg epoxy system has been fully characterised and the corresponding heat transfer model solution validated in [35]. For both RTM6 epoxy system and HexPly® M21 prepreg system the cure kinetics model is:

$$\frac{d\alpha}{dt} = k_1(1-\alpha)^{n_1} + k_2(1-\alpha)^{n_2}\alpha^m \tag{2}$$

$$k_i = \frac{1}{\frac{1}{k_{iC}} + \frac{1}{k_D}}, i = \{1,2\} \tag{3}$$

$$k_{iC} = A_i e^{\left(\frac{-E_i}{RT}\right)}, i = \{1,2\} \tag{4}$$

$$k_D = A_D e^{\left(\frac{-E_D}{RT}\right)} e^{\left(\frac{-b}{w(T-T_g)+g)}\right)} \tag{5}$$

Eq. (2) includes a catalytic and an autocatalytic term and two rate constants, k_1 and k_2. Kinetics models using a single rate constant achieve a limited accuracy in following the complex behaviour of cure reaction, models implementing two rate constants provide additional flexibility to follow the phenomenological cure kinetics behaviour; n_1, n_2 and m are reaction orders of the n-th order and autocatalytic term. Additionally, the model involves a diffusion term (k_D) which improves accuracy at later stages of the cure when the reaction becomes diffusion controlled; A_i, A_D are the Arrhenius pre-exponential coefficients for the chemical and diffusion dominated reaction,E_i, E_D the activation energies and b, *w* and g are constants. k_{iC} describes the chemical component of the rate constant defined in Eq. (4) where T is the absolute temperature, R the universal gas constant and α the degree of cure.

The evolution of the glass transition temperature depending on the degree of cure follows the DiBenedetto equation dependence for both RTM6 and HexPly® M21 epoxy systems [36]:

$$T_g = T_{g0} + \frac{(T_{g\infty} - T_{g0})\lambda\alpha}{1-(1-\lambda)\alpha} \tag{6}$$

where T_{g0} denotes the glass transition temperature of the uncured material, $T_{g\infty}$ the glass transition temperature of the fully cured material

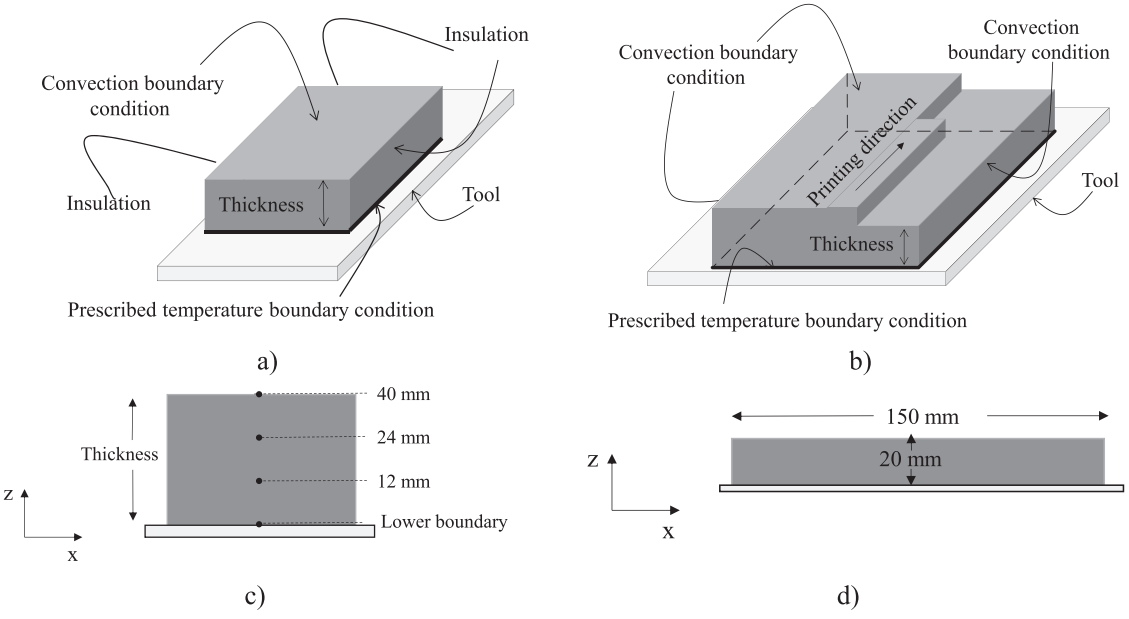

Fig. 1. Boundary conditions application: a) standard batch process; b) additive curing process; c) Case I, II, III and thickness direction; d) Case IV.

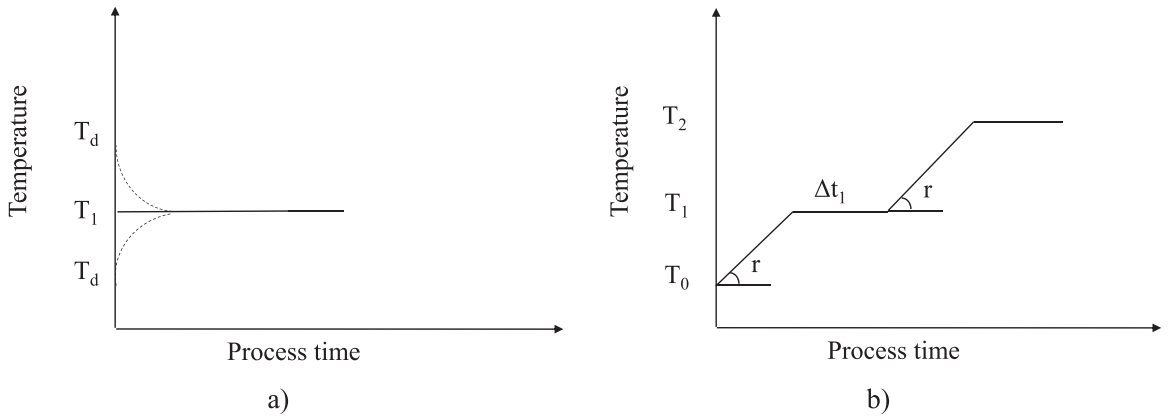

Fig. 2. Parameterised cure cycle: a) 3D printing scenario; b) standard batch process.

and λ is a fitting constant which controls the convexity of the non-linear dependence. The fitting parameters for the cure kinetics and Di Benedetto model for the two resin systems are reported in Table 2 [31] and 3 [35].

The specific heat capacity of the composite is computed using the rule of mixtures:

$$c_p = w_f c_{pf} + (1 - w_f) c_{pr} \tag{7}$$

where w_f is the fibre weight fraction, c_{pf} the specific heat capacity of the fibres and c_{pr} the specific heat capacity of the resin. The specific heat of carbon fibres follows a linear dependence on temperature [31,37]:

$$c_{pf} = A_{fcp} T + B_{fcp} \tag{8}$$

where A_{fcp} is the slope of the linear dependence and B_{fcp} the intercept. The specific heat capacity of both RTM6 epoxy and HexPly® M21 prepreg is described by a step function. The step change represents the transition of the resin from rubbery to glassy behaviour. Specific heat capacity depends on both temperature and degree of cure and is represented using the logistic function as follows [31,37]:

$$c_{pr} = A_{rc_p} T + B_{rc_p} + \frac{\Delta_{rc_p}}{1 + e^{C_{rc_p}(T - T_g - \sigma)}} \tag{9}$$

A_{rc_p} and B_{rc_p} are constants expressing the linear dependence of the specific heat capacity of the uncured epoxy on temperature and Δ_{rc_p}, C_{rc_p} and σ are the strength, width and temperature shift of the transition occurring at resin vitrification respectively.

The calculation of the thermal conductivity of the composite is based on the work of Farmer [38]:

$$K_{11} = v_f K_{lf} + (1 - v_f) K_r \tag{10}$$

$$K_{22} = K_{33} = v_f K_r \left(\frac{K_{tf}}{K_r} - 1\right) + K_r \left(\frac{1}{2} - \frac{K_{tf}}{2K_r}\right) + K_r \left(\frac{K_{tf}}{K_r} - 1\right) \sqrt{v_f^2 - v_f + \frac{\left(\frac{K_{tf}}{K_r} + 1\right)^2}{\left(\frac{2K_{tf}}{K_r} - 2\right)^2}} \tag{11}$$

where K_r, K_{lf} and K_{tf} are the thermal conductivity of resin and fibres in the axial and transverse direction respectively and v_f the volume fibre fraction. The thermal conductivity of carbon fibres in the axial (K_{lf}) and transverse directions (K_{tf}) is [34]:

$$K_{lf} = A_{lf} T + B_{lf} \tag{12}$$

$$K_{tf} = B_{tf} \tag{13}$$

Here A_{lf}, B_{lf} describe the linear dependence on temperature of longitudinal thermal conductivity of carbon fibres and B_{tf} the transverse. The thermal conductivity of the RTM6 resin depends on both temperature and degree of cure and is governed by the following expression [34]:

$$K_r = a_{Kr} T\alpha^2 + b_{Kr} T\alpha + c_{Kr} T + d_{Kr}\alpha^2 + e_{Kr}\alpha + f_{Kr} \tag{14}$$

Table 2
Parameters values for cure kinetics, specific heat and thermal conductivity constitutive models for the RTM6 epoxy resin system [31].

Cure Kinetics			Thermal conductivity			Specific heat		
Parameter	Value	Unit	Parameter	Value	Unit	Parameter	Value	Unit
A_1	17,580	s^{-1}	A_{lf}	0.0074	$Wm^{-1}°C^{-2}$	A_{fc_p}	0.0023	$Jg^{-1}°C^{-2}$
A_2	21,525	s^{-1}	B_{lf}	9.7	$Wm^{-1}°C^{-1}$	B_{fc_p}	0.765	$Jg^{-1}°C^{-1}$
A_d	$6.48 \bullet 10^{18}$	s^{-1}	B_{tf}	0.84	$Wm^{-1}°C^{-1}$	A_{rc_p}	0.0025	$Jg^{-1}°C^{-2}$
E_1	70,500	$Jmol^{-1}$	a_{Kr}	0.0008	$Wm^{-1}°C^{-2}$	B_{rc_p}	1.80	$Jg^{-1}°C^{-1}$
E_2	59,050	$Jmol^{-1}$	b_{Kr}	-0.0011	$Wm^{-1}°C^{-2}$	Δ_{rc_p}	-0.25	$Jg^{-1}°C^{-1}$
E_d	136,800	$Jmol^{-1}$	c_{Kr}	-0.0002	$Wm^{-1}°C^{-2}$	C_{rc_p}	1.10	$°C^{-1}$
m	1.16		d_{Kr}	-0.0937	$Wm^{-1}°C^{-1}$	σ	16.5	°C
n_1	1.8		e_{Kr}	0.22	$Wm^{-1}°C^{-1}$			
n_2	1.32		f_{Kr}	0.12	$Wm^{-1}°C^{-1}$			
b	0.467							
w	0.00048	$°C^{-1}$						
g	0.025							
T_{g0}	-11	°C						
$T_{g\infty}$	206	°C						
λ	0.435							

Here a_{Kr}, b_{Kr}, c_{Kr}, d_{Kr}, e_{Kr} and f_{Kr} are coefficients of the polynomial function. For the HexPly® M21 prepreg system, the measured K_{22} in [35] together with the reported fibre properties (Eqs. (12)–(13)) have been used to fit the following equation to define the thermal conductivity of the resin:

$$K_r = a_{Kr}T\alpha + b_{Kr}T + c_{Kr}\alpha + d_{Kr} \quad (15)$$

Table 2 and Table 3 report the values of parameters of the constitutive models described in Eqs. (2)–(15) for RTM6 and HexPly® M21 systems respectively [31,35].

3. Optimisation methodology

A meaningful way to compare the performance of the two manufacturing routes considered (i.e. standard vs 3D printing) is to identify optimal solutions for the two processes with respect to the same parameters and objectives and quantify the outcomes. The comparison based on the comprehensive simulation of the cure was carried out for the case of the Liquid Composite Moulding (LCM) system considered in this work (RTM6/carbon fibre). The objectives selected to base the analysis on are process time (t_{proc}) and maximum temperature overshoot (ΔT_{max}). The first objective drives the cost of the process, whilst the second relates to the quality of the component as it can be linked to residual stresses and spring-in/warpage formation [20] as well as potential exothermic effects. Both objectives are related to the sustainability of the process as minimising process time means reducing energy consumption and minimising the temperature overshoot implies better quality and reduction of scrap rate. Moreover, a constraint of a maximum allowed temperature of 200 °C has been added to eliminate any risk of resin degradation. The constraint could be relaxed in order to shift the Pareto fronts towards shorter processing time and higher temperature overshoots. This is a conservative choice since the degradation onset temperature of RTM6 is about 300 °C [39]. For the 3D printing process, a constraint of maximum degree of cure for an existing layer upon which deposition of the newly material occurs has been set to 0.59, which corresponds to the gelation point for RTM6 [40]. The constraint is therefore, violated when a new layer is placed on top of an element that has a degree of cure greater than 0.59. This choice is supported by the fact that interfacial properties are retained between layers if gelation of the underlying layer does not occur prior to deposition [19]. The parameters of the optimisation problem for the conventional batch process are the ramp rate (r), duration of first dwell (Δt_1), temperature of first (T_1) and second (T_2) dwell. The second dwell duration (Δt_2) is not considered as an optimisation parameter since the objective t_{proc} is defined as the time at which the minimum degree of cure reached in the model is 0.88, which is the maximum degree of cure achieved when undergoing a DSC isothermal test at the standard cure temperature of 180 °C of the RTM6 resin [31]. The overshoot is defined as the maximum temperature difference between any given location of the model and the prescribed temperature boundary condition throughout the process duration. For the 3D printing scenario, the deposition temperature (T_d), dwell temperature (T_1) and printing speed (v) are the three optimisation parameters. Table 4 reports the ranges selected for each parameter. The temperature ranges chosen are driven by the nature of the cure kinetics of the systems with standard batch process implementing a more conservative range due to the tendency to overshoot; the printing speed was selected according to current printing speed achieved in the printing of continuous reinforced thermosetting composites [41]. Fig. 2 illustrates the two-dwell cure cycle adopted in the 3D printing and standard batch process scenarios.

The multi-objective optimisation problems are formulated as follows:

For batch processing:

$$\{r, \Delta t_1, T_1, T_2\} = \underset{subject\ to T < 200℃}{\text{argminh}}\left(\Delta T_{max}(r, \Delta t_1, T_1, T_2), t_{proc}(r, \Delta t_1, T_1, T_2)\right) \quad (16)$$

and for 3D printing:

$$\{v, T_1, T_d\} = \underset{subject\ to T < 200℃ and \alpha_{underlying} < 0.59}{\text{argming}}\left(\Delta T_{max}(v, T_1, T_d), t_{proc}(v, T_1, T_d)\right) \quad (17)$$

Hereh : $R^2 \rightarrow R$ and g : $R^2 \rightarrow R$ are arbitrary functions non-decreasing in their arguments and $\alpha_{underlying}$ is the degree of cure of the existing layer underlying the location of deposition in 3D printing. Use of Eqs. (16), (17) for all non-decreasing functions h and gmeans that there are multiple solutions for each problem which form the corresponding Pareto fronts comprising efficient solutions **x** for which there is no other solution **x′** that satisfies $(\Delta T_{max}(\mathbf{x}') \leq \Delta T_{max}(\mathbf{x})$and $t_{proc}(\mathbf{x}') < t_{proc}(\mathbf{x}))$ or $(\Delta T_{max}(\mathbf{x}') < \Delta T_{max}(\mathbf{x})$and $t_{proc}(\mathbf{x}') \leq t_{proc}(\mathbf{x}))$. Therefore, for each efficient solution of the two objective problem there is no other solution that is better with respect to one objective without being worse with respect to the other objective. This multi-objective setting allows

Table 4
Design parameters ranges.

Standard batch process		3D printing process	
Parameter	Range	Parameter	Range
T_1(℃)	145–175	T_d(℃)	165–195
T_2(℃)	175–195	T_1(℃)	165–195
Δt_1 (s)	100–4500	v(mm/min)	50–600
r(℃/min)	1–4		

Table 3
Parameters values for cure kinetics, specific heat and thermal conductivity constitutive models for the HexPly® M21 prepreg system [35].

Cure Kinetics			Thermal conductivity			Specific heat		
Parameter	Value	Unit	Parameter	Value	Unit	Parameter	Value	Unit
A_1	420,615	s^{-1}	A_{lf}	0.0074	$Wm^{-1}℃^{-2}$	A_{fc_p}	0.00205	$Jg^{-1}℃^{-2}$
A_2	57,440	s^{-1}	B_{lf}	9.7	$Wm^{-1}℃^{-1}$	B_{fc_p}	0.75	$Jg^{-1}℃^{-1}$
A_d	$2.6 \bullet 10^{20}$	s^{-1}	B_{tf}	0.84	$Wm^{-1}℃^{-1}$	A_{rc_p}	0.0029	$Jg^{-1}℃^{-2}$
E_1	78,890	$Jmol^{-1}$	a_{Kr}	-0.00349	$Wm^{-1}℃^{-2}$	B_{rc_p}	1.84	$Jg^{-1}℃^{-1}$
E_2	68,978	$Jmol^{-1}$	b_{Kr}	-0.00134	$Wm^{-1}℃^{-2}$	Δ_{rc_p}	-0.26	$Jg^{-1}℃^{-1}$
E_d	87,456	$Jmol^{-1}$	c_{Kr}	0.826	$Wm^{-1}℃^{-1}$	C_{rc_p}	0.15	$℃^{-1}$
m	0.6		d_{Kr}	0.531	$Wm^{-1}℃^{-1}$	σ	0.65	℃
n_1	0.8							
n_2	3.2							
b	1.98							
w	0.000165	$℃^{-1}$						
g	0.058235							
T_{g0}	1.5	℃						
$T_{g\infty}$	194	℃						
λ	0.67							

considering the two objectives independently, without prioritising their relative importance a priori by using weights through a prescribed form of functions h and g.

A Genetic Algorithm (GA) capable of addressing multi-objective problems has been adapted and linked to the commercial software Abaqus®. The GA implementation has been successfully tested against reliability and robustness benchmark problems and real case optimisation problems [8,31,37]. An interface has been developed in C+ + to link the GA and the commercial software Abaqus® as illustrated in Fig. 3. The operation of interface is as follows. A template input file is generated by Abaqus® FE. At each function execution, the interface generates a new input file inserting the new initial temperature, and updates the cure cycle parameter values and process speed in the case of 3D printing in the DISP, FILM and UEPACTIVATIONVOL user subroutines. Subsequently, the interface runs the Abaqus® simulation with the newly generated input file and user subroutines. The simulation uses user subroutines UVARM and UEXTERNALDB to obtain the temperature and degree of cure at each node and element. The maximum temperature difference between the lower boundary and the interior model is stored and updated, whilst another variable updates the minimum degree of cure at the end of each step. As soon as the minimum degree of cure in the model reaches 0.88, the values of process t_{proc} and ΔT_{max} are stored in a text file and read by the interface to pass on to the Pareto front array. At this point a new set of parameters is made available by the GA and a new individual solution begins. The GA is executed in generations of individuals, with reproduction operations used to produce new individuals forming a new generation based on the performance of the current generation member. The algorithm is executed until no significant further improvement is visible in the Pareto solutions. Table 5 reports the values of the parameters of GA used for the optimisation problem. Each generation of the GA comprised 40 individual representing the potential solutions, with the top 32 individual utilised in reproduction. The probability of cross-over during reproduction was set at 50 %, with a small mutation probability of 0.5 % allowing local refinement of the solution.

Table 5
Optimisation parameters values.

Parameters	Values
Population individuals	40
Reproduction individuals	32
Elite individuals	4
Cross-over probability	50 %
Mutation probability	0.5 %

4. Results and discussion

In the following, Section 4.1 presents a comparison between the curing behaviour in a batch and a 3D printing process in the case of the LCM system (RTM6 epoxy/carbon fibre); in this section, Manufacturer Recommenced Cure Cycles (MRCCs) are used for the analysis in the context of standard manufacturing practice. Section 4.2 presents and discusses the results of the optimisation with respect to the thermal profile used, whilst Section 4.3 introduces a simplified model analysis based on data collected from FE runs using for the LCM (RTM6 epoxy/carbon fibre) system. In Section 4.4 the simplified analysis is extended to the case of a prepreg system with analysis of 3D printing of the HexPly® M21 prepreg system.

4.1. Comparison of batch and additive process for the Liquid Composite Moulding system

Fig. 4 shows the temperature distribution for the standard batch process for Case III at different process times (Fig. 4a) whilst Fig. 4b illustrates the evolution at four different locations: the lower boundary, 12 mm and 24 mm and 40 mm across the thickness (as shown in Fig. 1c). The two MRCCs proposed for RTM6 [23,31] lead to a violation of the 200 °C maximum allowed temperature for the component thickness considered here. Therefore, a variation of the latter has been used here to illustrate the evolution of the cure. This profile involves a first dwell at 150 °C instead of the standard 160 °C used in the MRCC [31]. The outer layers of the material heats up first due to the contact with the tool and convection at the top. However, after a certain time, the cure reaction and its exothermic effects become dominant and the central part reaches higher temperature than the boundaries (at 5150 s in Fig. 4a). This is manifested as a temperature overshoot, which can be detrimental for the quality and mechanical performance of the final component and should be minimised [8,20,31]. The temperature overshoot reached in the standard batch process (Fig. 4b) is about 50 °C with

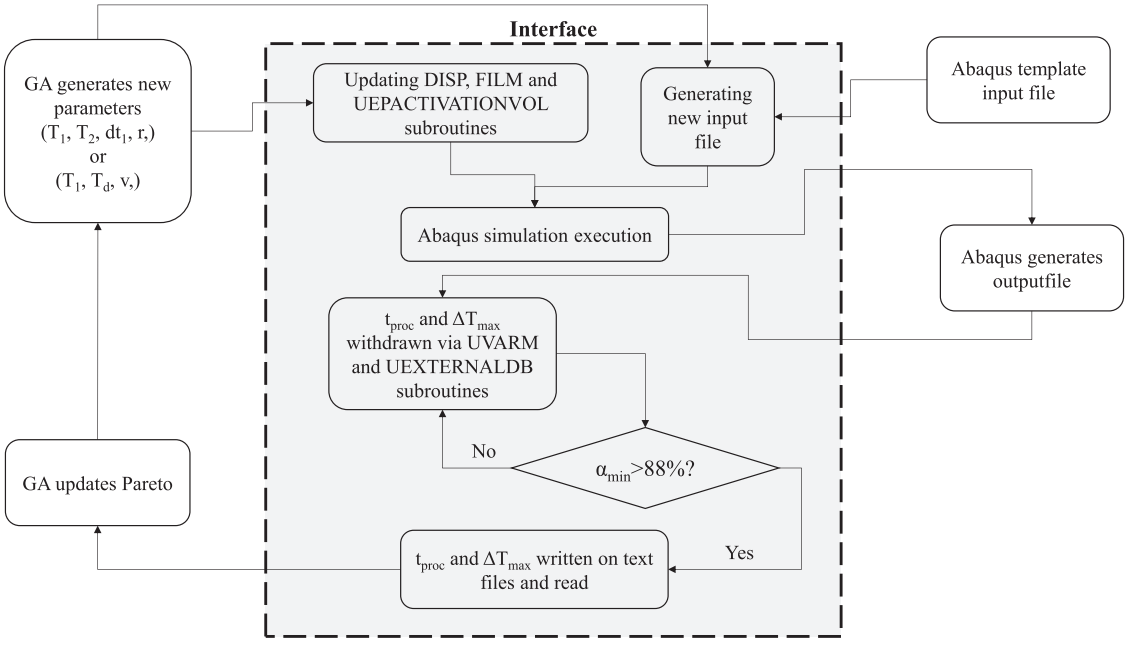

Fig. 3. Functioning of the interface linking Abaqus® FE and the GA.

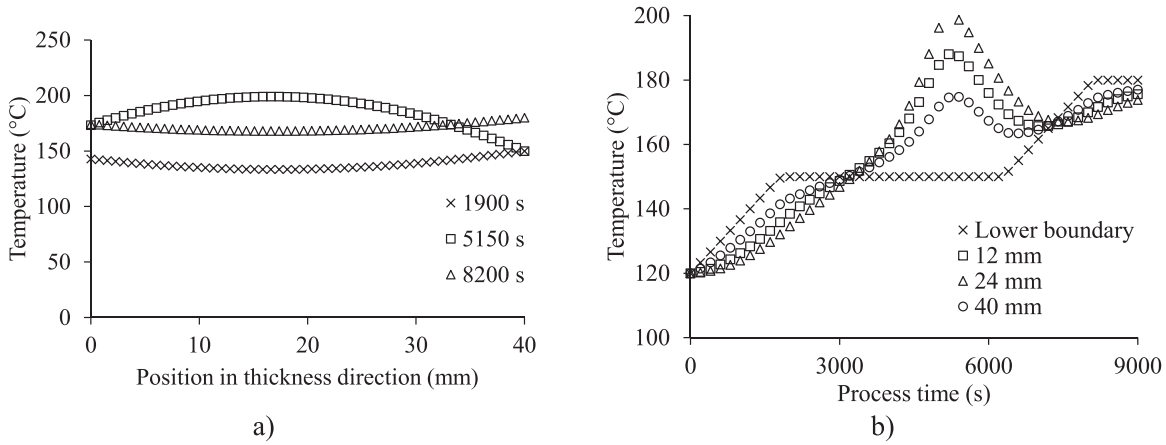

Fig. 4. Temperature across thickness for the RTM6 epoxy/carbon fibre system when the modified MRCC is applied a) distribution across the thickness direction at different processing times; b) evolution at fixed positions.

a process time of 8200 s. Once the maximum temperature overshoot is reached at about 5150 s, the reaction becomes slower as most of the chemical potential of the resin has been converted to network formation. Fig. 4b shows that the part still has a 10 °C temperature gradient across its thickness at the time the process ends when a minimum degree of cure of 0.88 is reached.

Fig. 5 illustrates the degree of cure distribution for the standard batch process for Case III at different process times (Fig. 5a) whilst Fig. 5b reports the evolution at four different locations: the lower boundary, 12 mm and 24 mm and 40 mm across the thickness. At the time of maximum temperature overshoot (at 5150 s), the degree of cure across the thickness is higher than the gelation degree of cure of RTM6 (0.59). This behaviour is not desirable in the generation of cure induced residual stresses, since a high temperature gradient across the thickness exists past the gelation point when stresses cannot relax instantaneously anymore due to the formation of a cross-linked 3D network. The degree of cure evolution in Fig. 5b reflects the temperature evolution reported in Fig. 4b. The evolution is typical of an inside out curing scenario where the middle part experiencing temperature overshoot cures faster than the boundaries.

Fig. 6 illustrates the temperature distribution for the 3D printing process for Case III at different process times (Fig. 6a), Fig. 6b illustrates the evolution at three different locations and at points located at the lower boundary, 12 mm and 24 mm and 40 mm across the thickness for the case of the printing head kept at 150 °C, the tool/bed kept at 180 °C, and printing speed of 100 mm/min; Fig. 6c illustrates the temperature contour plot at 4900 s. The locations selected are in the axis of symmetry. The material at 12 mm is deposited after about 1400 s, at 24 mm after around 2800 s and at 40 mm after 4700 s. The additive manufacturing nature of the process allows to contain the temperature overshoot of the component during the deposition while progressing the cure in a safe manner (Fig. 6a). Although the case shown in Fig. 6 is a not an optimised solution, the benefits of 3D printing compared to standard batch process are noticeable, as the maximum temperature overshoot in the component is 4 °C (Fig. 6a) which is 44 °C less than the value obtained with conventional batch processing. Furthermore, the process is completed after 6900 s which corresponds to an 18 % process time reduction with respect to the conventional batch process with no observable temperature gradient across thickness. These features are also reflected in the temperature evolution during the process at the different locations reported in Fig. 6b.

Fig. 7 depicts the degree of cure distribution for the 3D printing process for Case III at different process times (Fig. 7a) whilst Fig. 7b reports the history at the four locations examined (lower boundary, 12 mm and 24 mm and 40 mm). Fig. 7c illustrates the degree of cure contour plot at 4900 s. In Fig. 7a, as deposition is still in progress, the bottom part of the component has already cured up to 0.92. By the time the maximum temperature difference occurs, most of the component is already cured. This has the beneficial effect of reducing exothermic effects since only a fraction of the part is at a low degree of cure with the chemical reaction playing a role with the rest of the material having most of its reactivity already consumed. The final degree of cure across the thickness is in the range of 0.89–0.93, with only the very last deposited material lagging behind. If the part is left an additional 600 s the range would be 0.91–0.93. In Fig. 7b, the degree of cure evolution shows no differences either in the rate or in the final degree of cure

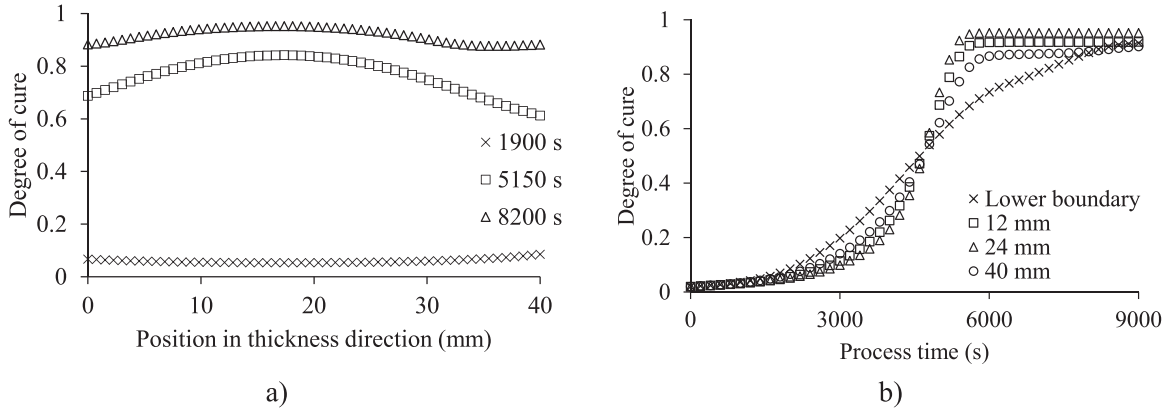

Fig. 5. Degree of cure across thickness for the RTM6 epoxy/carbon fibre system when the modified MRCC is applied a) distribution across the thickness direction at different processing times; b) evolution at fixed positions.

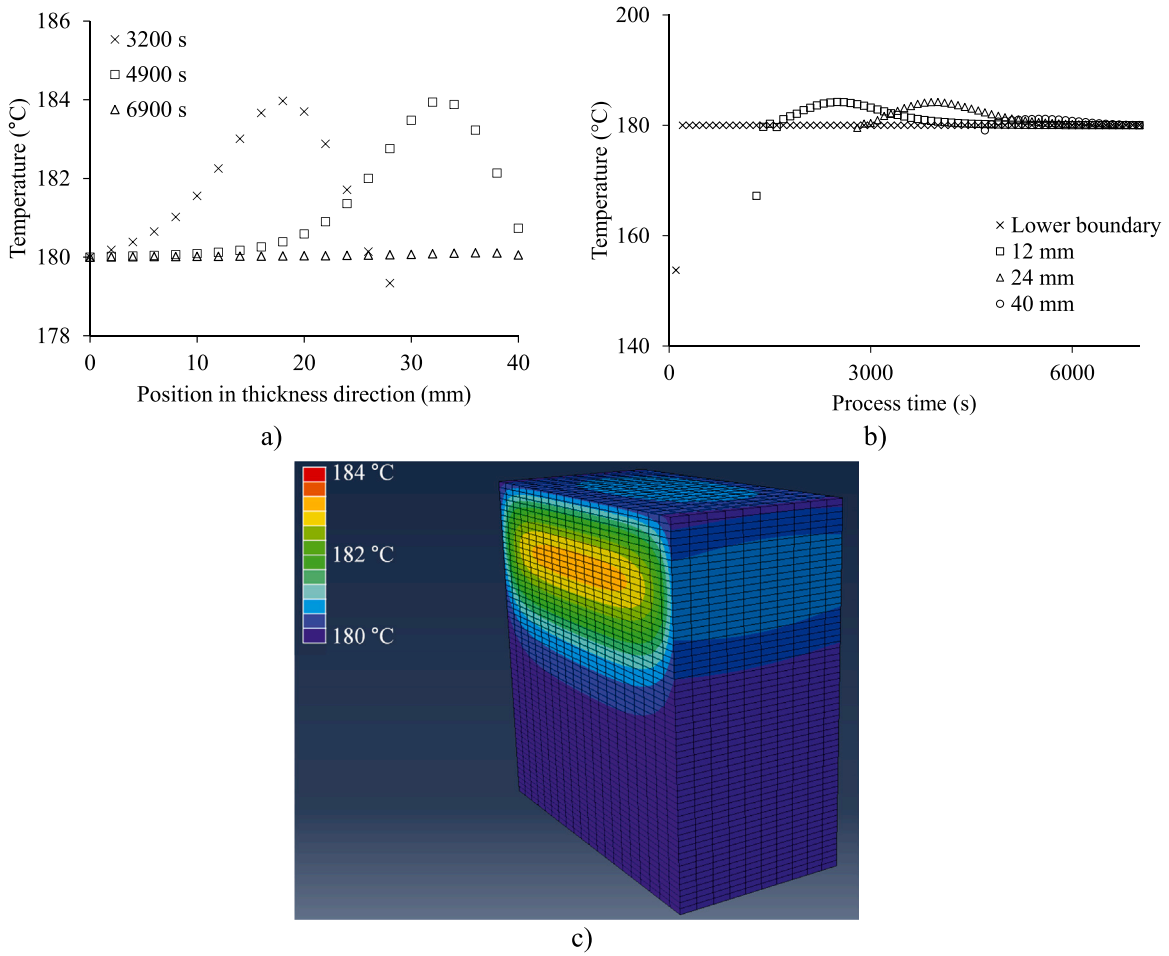

Fig. 6. Temperature distribution for the 3D printing process of the RTM6 epoxy/carbon fibre system when modified MRCC is a) distribution across the thickness direction at different processing times; b) evolution at fixed positions; c) contour plot at 4900 s.

achieved, guaranteeing homogenous curing across thickness.

4.2. Batch and 3D printing process optimisation for the Liquid Composite Moulding system

Fig. 8 presents a comparison of the Pareto fronts obtained by the multi-objective optimisation for Case I, II and III using 3D printing and standard batch processing of the RTM6 epoxy/carbon fibre system. The GA converges to the Pareto fronts after 4 generations in all three 3D printing cases taking approximately 16, 18 and 21 h computational time to complete the solution for the 20, 30 and 40 mm case respectively on a standard desktop PC equipped with an Intel® Core ™ i7–4790 CPU @ 3.6 GHz processor. A fixed time step of 30 s has been chosen for the 3D printing process, which allows quantifying the process time objective with an accuracy of ± 15 s since each increment lasts 30 s. The convergence for the standard process required 10, 15 and 20 generations respectively for Case I, II and III highlighting the additional complexity of the cure problem for a batch process (i.e. oven). Although the optimisation required more function evaluations to converge, the adaptive time step made the simulation faster (i.e. about two minutes per individual solution); therefore the final Pareto fronts were reached in about 13, 20, 27 h computational time for Case I, II and III respectively. The six Pareto fronts show the characteristic L-shape trade-off of the two objectives selected [8,31]. The L-shape of the fronts highlights the competitive nature of the two objectives. Two regions can be identified: a vertical region in which process time is prioritised and the process designer can achieve significant improvements in temperature overshoot; and a horizontal region where the temperature overshoot objective is prioritised and significant reduction in process time is possible. Corner solutions are ideal candidates for applications, as they tend to achieve a good compromise without entering extreme scenarios with respect to any of the two objectives. Details of the design parameters of solutions belonging to different regions of the Pareto front for the four configurations are reported in Table 6. Solutions in close proximity in the objective space do not necessarily stand close in the design space and very different combinations of design parameters might lead to neighbouring solutions. This is possible for non-linear optimisation problems with a complex landscape [31]. In the problem addressed here, the added complexity comes from the non-linearity of the exothermic process that facilitates the appearance of local minima in the objective space. The dependence of the Pareto front on thickness for standard batch processing shows strong non-linearity which confirms previous findings [8]. The non-linearity is the result of the temperature dependence of cure kinetics evolution and the low through thickness thermal conductivity of thermosetting matrix composite materials.

The Pareto front solution for batch processing allows a reduction of up to 60 % in process time and up to 50 % in temperature overshoot compared to the Manufacturer Recommended Cure Cycle (MRCC) [8,31]. The application of MRCC [23] leads in all three cases to a violation of the 200 °C maximum temperature constraint; therefore a meaningful comparison with optimised results cannot be established. The results reported in Fig. 8a show that by manufacturing the composite components via 3D printing, a reduction in process time of 45 %, 48 % and 52 % and 65 %, 76 % and 85 % in temperature overshoot is achieved for Case I, II and III respectively compared to optimal solutions for batch processing. Furthermore, the dependence of temperature overshoot on

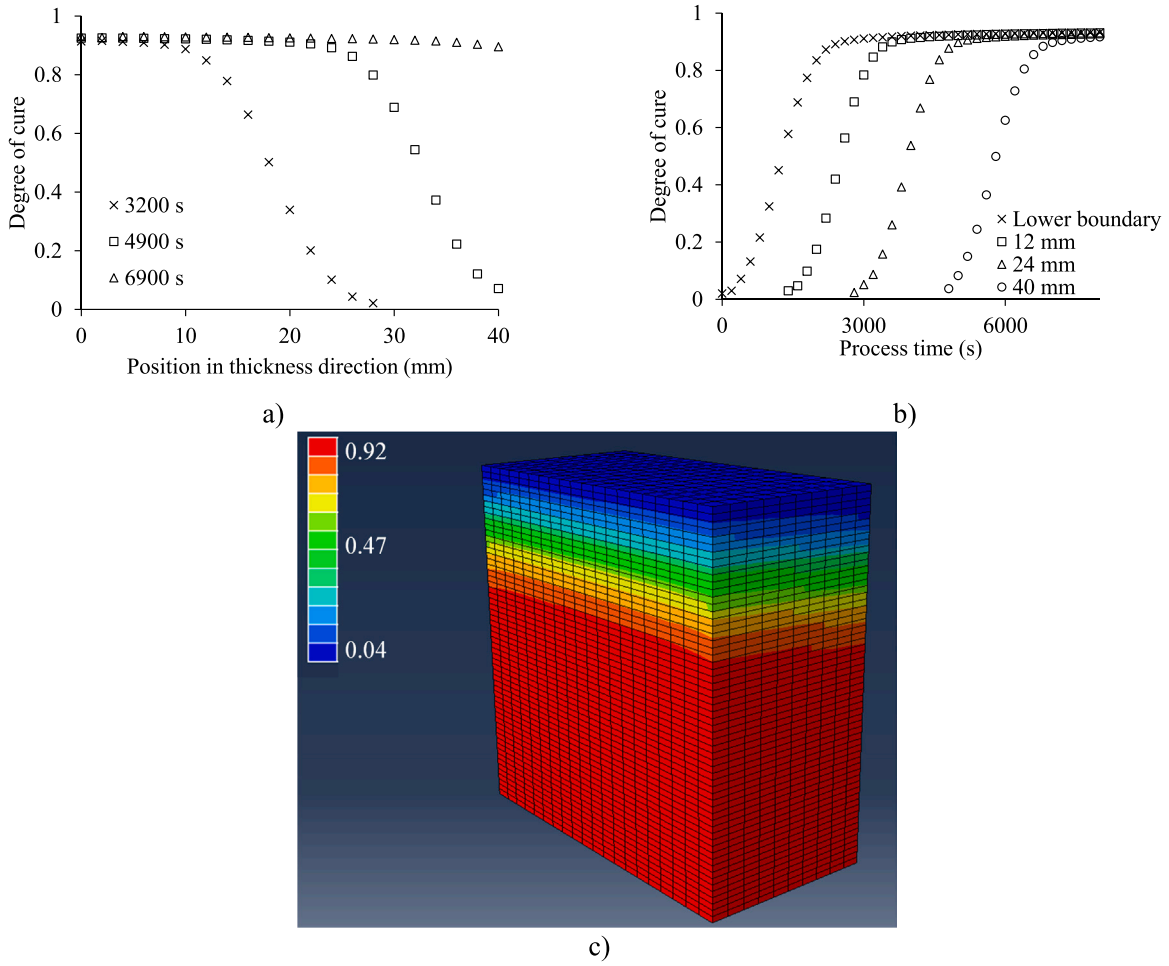

Fig. 7. Degree of cure distribution for the 3D printing process of the RTM6 epoxy/carbon fibre system when a modified MRCC is applied a) distribution across the thickness direction at different processing times; b) evolution at fixed positions; c) contour plot at 4900 s.

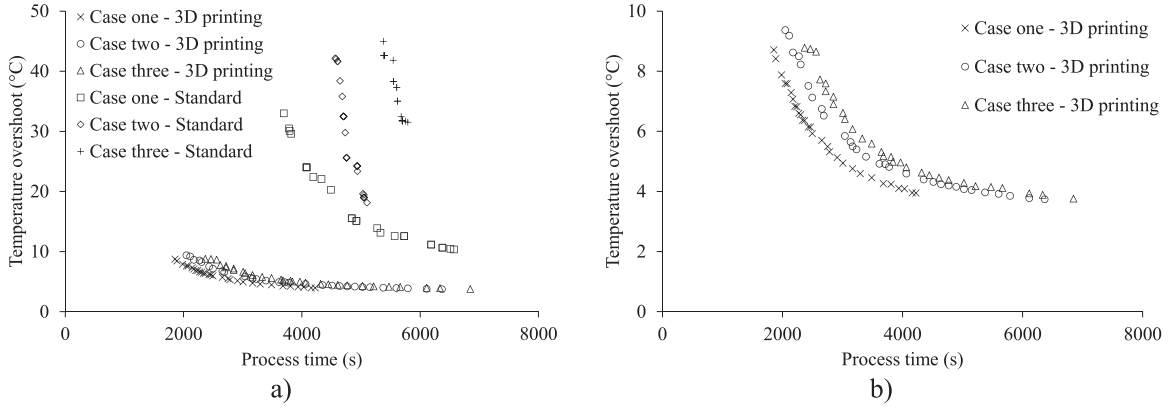

Fig. 8. Pareto fronts comparison for the RTM6 epoxy/carbon fibre system: a) 3D printing and standard batch process; b) detailed view of the 3D printing Pareto fronts.

thickness is made negligible in 3D printing by the additive nature of the process. Once the process reaches a steady state, each new layer deposited undergoes the same thermal history and therefore from this point onward manufacturing thicker components does not increase the temperature overshoot. This result highlights the inherent advantage of an additive process and its potential for overcoming current limitations in geometry of parts that can be manufactured using thermosetting matrix composites. The three fronts of the 3D printing process in Fig. 8b have similar temperature overshoot spanning from 4 °C to 9 °C, whilst process time ranges at about 2000–6000 s

Fig. 9 illustrates the comparison for the 20 mm thick case between the 3D printed 40 mm long component, the 3D printed 150 mm long component and standard batch manufacturing process (i.e. Case I and IV). The optimisation of the 150 mm long component (i.e. Case IV) converged after 4 generations and took about 10 h computational time to complete. Although the 150 mm long component has dimensions

Table 6
Design parameters of Pareto individuals for the RTM6 epoxy/carbon fibre system in the corner, vertical and horizontal regions of the front for the different configurations.

Case	Solution		Design parameters						Objectives	
			T_1(℃)	T_2(℃)	Δt_1(s)	r(℃/min)	T_d(℃)	v(mm/min)	ΔT_{max}(℃)	t_{proc}(s)
I	Vertical	3D printing	190				189	583	8.2	1900
		Batch process	167	185	2248	3.8			32	3555
	Corner	3D printing	176				184	583	4.9	2944
		Batch process	162	182	1797	1.7			24	4293
	Horizontal	3D printing	170				177	600	3.9	4128
		Batch process	146	182	3322	1.3			11	6400
II	Vertical	3D printing	188				173	552	8.3	2272
		Batch process	155	195	3287	3.7			40	4605
	Corner	3D printing	173				166	600	4.9	3616
		Batch process	150	182	3287	3.8			26	4757
	Horizontal	3D printing	166				176	539	3.7	6100
		Batch process	149	182	2733	1.8			18	5100
III	Vertical	3D printing	188				168	513	8.6	2560
		Batch process	149	194	3980	3.5			45	5400
	Corner	3D printing	173				184	522	4.9	3936
		Batch process	145	185	4119	3.6			33	5750
	Horizontal	3D printing	166				173	578	3.7	6560
		Batch process	145	186	3980	2.8			31	5791
IV	Vertical	3D printing	192				167	578	6.6	3120
	Corner	3D printing	181				174	557	5.1	3840
	Horizontal	3D printing	171				168	327	3.3	6240

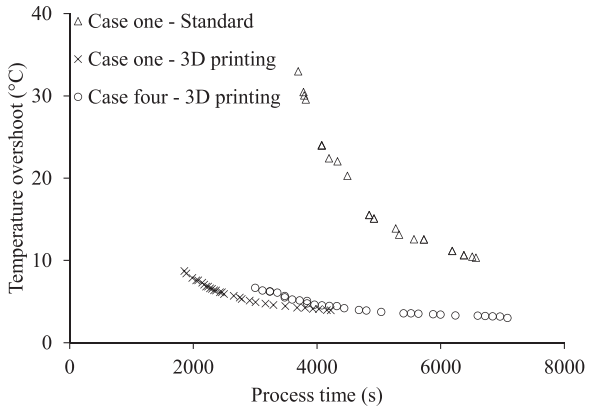

Fig. 9. Pareto fronts comparison for the RTM6 epoxy/carbon fibre system between 20 mm thick components, 3D printed and standard batch manufacturing.

almost four times greater, the increase in process time in the optimal Pareto points is about 1000 s offering about 35 % process time reduction compared to standard batch manufacturing Pareto. On the other hand, the benefits in terms of temperature overshoot reduction are unchanged compared to the 40 mm long component. The majority of individuals in the final Pareto set have a printing speed higher than 400 mm/min. This means that shorter process times are possible depending on the printing speed that 3D printing can achieve.

The outcome of the optimisation can be explained by examining in detail the evolution of temperature at different locations across the thickness of the component. Since thickness is the main driver of exothermic effects leading to potential detrimental thermal gradients, Case III has been selected for further analysis and one corner solution from the Pareto front has been highlighted for each scenario. As observed in Table 6, the temperature of the first dwell in the standard batch process decreases in search for milder reaction, nevertheless resulting in increasing temperature overshoot as thickness increases. This does not occur in the 3D printing scenario. Fig. 10 reports the temperature history of four different locations (i.e. lower boundary, 12, 24 and 40 mm in the thickness direction as shown in Fig. 1c) for the 3D printing process and the standard batch process. Case III corner solutions in Table 6 are considered here. Fig. 10a shows a drop in temperature at the time at which new material is deposited after about 260, 520 and 900 s. Consequently, large thermal gradients in the through thickness directions are reduced as the results in Table 6 highlight. In light of this,

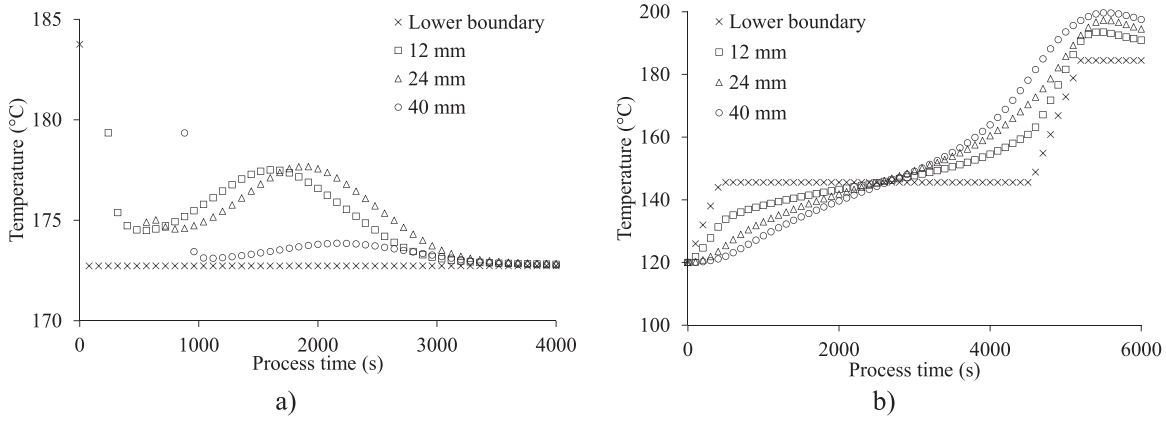

Fig. 10. Thermal history at four different locations through thickness for the two Case III corner solutions reported in Table 6 for the RTM6 epoxy/carbon fibre system: a) 3D printing process; b) standard batch process.

slower printing does not necessarily lead to lower exothermic reaction. There is a trade-off between progressing the cure in one layer to reduce the chemical potential of the resin and the cooling effect due to deposition of colder material. This is due to a combination of the shift in reaction rate and temperature peaks due to the additive nature of the process which has beneficial effects in containing the overall overshoot and the lower boundary mitigating overshoot by being at a lower temperature level throughout the process. Additive curing is exploiting the consumption of the chemical potential of the resin gradually at a fraction of the total thickness; this contributes to less heat generation at the centre of the component and a better route for the dissipation of the heat generated. In contrast to this behaviour, Fig. 10b highlights that during the first dwell and ramp of the batch process, the temperature increases reaching a maximum difference of 35 °C. Furthermore, a significant overshoot occurs in the second dwell. This overshoot occurs after the part has already passed the gelation point and stress cannot therefore relax quickly. As a consequence of this thermal behaviour, the curing process for a 3D printing strategy can be designed with more aggressive first dwell temperatures (172 °C) whilst the standard batch cure process needs to adopt milder temperatures (145 °C), still obtaining worse results.

Fig. 11 illustrates the degree of cure evolution at four different locations across the thickness for the two Case III corner solutions reported in Table 6. Fig. 11b shows the typical behaviour of a thick component that generates exothermic effects which invert the thermal gradient from an outside in to an inside out curing. As opposed to this evolution, Fig. 11a presents a much more homogenous evolution for the different layers. All locations follow a similar degree of cure evolution, only shifted forward in time for positions closer to the upper surface of the component. This behaviour allows avoiding intense exothermic effects and makes the manufacturing of thick and ultra-thick components feasible with very low temperature overshoot. Furthermore, the manufacturing of thick and ultra-thick components using 3D printing follows the same trends in degree of cure evolution as those of thin components without a crossover point after which the interior of the laminate starts curing faster than the outer layers. The component manufactured with 3D printing ends with a homogenous final degree of cure of 0.89 across the thickness, whilst the component manufactured with a standard batch process has a range of final degree of cure of 0.90–0.95, which is a source of additional residual stresses and macroscopic inhomogeneity. It can be observed in Fig. 11a that when the last layer of material is deposited at 40 mm, the first layer of material has reached a degree of cure of 0.2, the layer at 12 mm has cured to about 0.15 and the layer at 24 mm has reached about 0.1 degree of cure. This degree of cure evolution allows the retention of interfacial properties while containing exothermic effects since at the time the overall thickness is reached, part of the chemical potential of the resin has been consumed.

Fig. 12 depicts the reaction rate evolution at the four different locations (boundary, 12, 24 and 40 mm) for the two Case III corner solutions reported in Table 6. The two processes reach similar levels of maximum reaction rate. However, the occurrence of maximum rate is distributed over time in the additive process, thus minimising the rate of heat release. In contrast, in the batch process, the occurrence of a maximum reaction rate is within a narrow time range (4500–5000 s) for the different locations, generating a cumulative heat release effect that is far stronger and can cause a significant overshoot.

4.3. Exploration of 3D printing process outcomes of the Liquid Composite Moulding system based on simplified process model

The additive nature of the 3D printing process results and the moderation of the non-linear character of the cure process generates an opportunity for efficient approximation of process outcomes through simplified modelling. This can facilitate a wide and exhaustive investigation of how the 3D printing process can address different component geometries. Furthermore, it can form the basis for fast optimisation – for example selection of process speed and tool temperature – carried out at a component level as part of process setup.

The total process duration can be decomposed into two parts: (i) the time required to deposit the impregnated tow; and (ii) the time required to cure the last material deposited during 3D printing. The deposition time can be approximated as total volume of the work piece divided by material flow rate computed as the product of printing speed to cross section area of the tow:

$$t_{printing} = \frac{Vol}{vA_t} \tag{18}$$

Here Vol is the component volume, v the printing speed and A_t the deposited tow cross sectional area. Approximation of the time required to cure the last material deposited can be carried out based on an assumption of constant temperature equal to the tool/oven temperature of the process (T_1). This assumption is justified by the low overshoots observed and their local and transient character as reported in Section 4.2. Under this assumption, the cure kinetics model described by Eqs. (2)–(5) can be used to compute the time required to reach the final degree of cure, which is 0.88 in the case of the RTM6 epoxy system. Cure time can be expressed as follows:

$$t_{cure} = f_{T_1}^{-1}(\alpha_f) \tag{19}$$

where $f_{T_1}(t)$ is the integral of the cure kinetics model calculated numerically using Eqs. (2)–(5) at a constant temperature T_1 yielding the evolution of degree of cure as a function of time (t) and $f_{T_1}^{-1}(\alpha_f)$ its

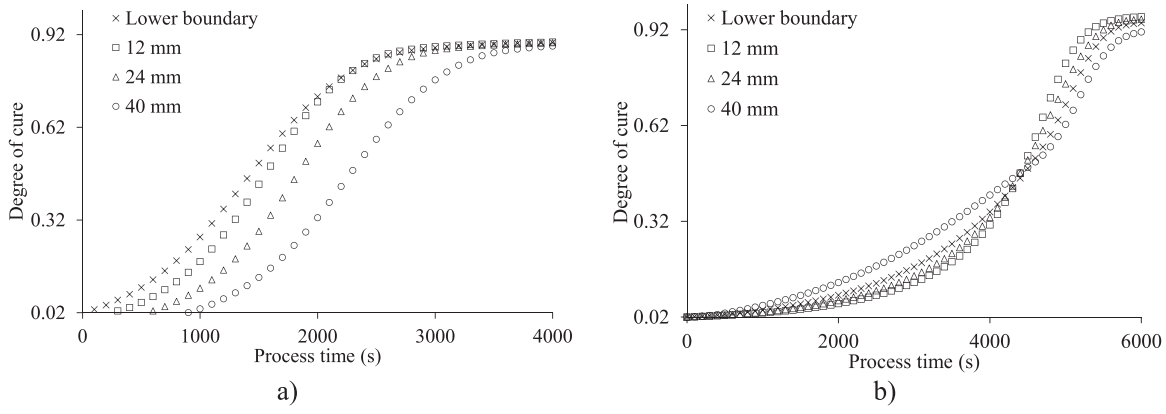

Fig. 11. Degree of cure history at four different locations through thickness for the two Case III corner solutions reported in Table 6 for the RTM6 epoxy/carbon fibre system: a) 3D printing process; b) standard batch process.

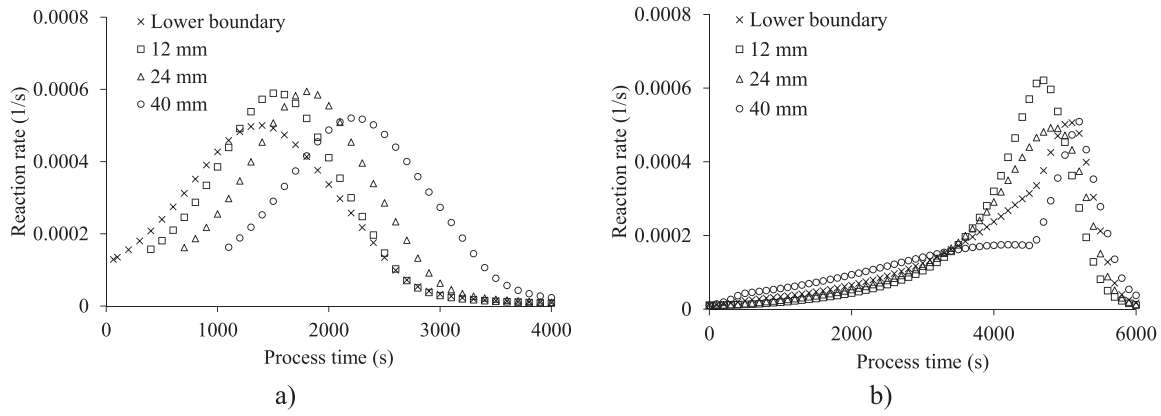

Fig. 12. Reaction rate history at four different locations through thickness for the two Case III corner solutions reported in Table 6 for the RTM6 epoxy/carbon fibre system: a) 3D printing process; b) standard batch process.

inverse expressing the time required to reach the final degree of cure (α_f).

The overall process duration approximation can be expressed as:

$$t_{proc} = t_{printing} + t_{cure} = \frac{Vol}{vA_t} + f_{T_1}^{-1}(\alpha_f) \tag{20}$$

Eq. (20) and the parameter values of the cure kinetics model reported in Table 2 have been used to compute an approximate process duration for all the points of the Pareto fronts of the 3D printing process reported in Figs. 8 and 9. The results are set against the process duration computed by the FE model in Fig. 13a. It can be observed that the results of the two computations are almost identical. The simplified model overestimates very slightly the process duration by 50–200 s as a result of the isothermal assumption which does not account for the transient acceleration of the reaction resulting from the small temperature overshoot predicted by the FE simulation. The difference is negligible and has no practical effect to the estimation of 3D printing process outcomes.

The temperature overshoot observed during 3D printing is not influenced significantly by the component thickness due to the additive character of the process as discussed in Section 4.2. Furthermore, the in-plane dimensions of the printed component have a limited influence to the overshot observed, following from the fact that dissipation of heat tends to happen in the through thickness direction purely due to its different scale compared to in-plane dimensions. This effect is shown in Fig. 13b, which illustrates the temperature overshoot versus tool/oven temperature for all the Pareto front points reported in Figs. 8 and 9. A strong correlation exists indicating a linear dependence. For the range of cases considered here the approximation is:

$$\Delta T_{max} = 0.196 T_1 - 29.22 \tag{21}$$

where both temperature overshoot and tool/oven temperature are in °C. The approximation, which is applicable to the material combination used here and a range of tool/oven temperature of 165–190 °C. Eq. (21) has a maximum error of about 2 °C. The cause of this is around variations of heat dissipation in the in-plane direction - especially in the direction of the fibres – causing some influence of the side boundary condition on the temperature overshoot. This is of limited importance in terms of practical aspects of the process, as the effect of this error on process strains as well as potential degradation estimates is very small. The linear dependence shown in Eq. 21 shows that a relaxation in the maximum temperature constraint would translate linearly in temperature overshoot variation.

The approximation expressed by Eqs. (20) and (21) can be used directly to approximate the Pareto front for a component of given volume. This is carried out by minimising the duration of deposition through maximisation of printing speed within the range allowed and computation of the cure duration and temperature overshoot for every tool/oven temperature within the range of the optimisation. This approach, which uses fully the linearity of printing and ignores intricacies of the process around the interaction between printing head and work piece temperature as well as in-plane heat dissipation effects, establishes in a very simple calculation the range of process durations that can be achieved as a function of temperature overshoot that can be tolerated. The overall quality of this approach is illustrated in Fig. 14 which compares the Pareto fronts obtained using the FE cure simulation and reported in Figs. 8 and 9 with the results of the approximate analysis for a wide range of tool oven temperature of 150–200 °C. The simplified solution reproduces successfully the range of the two objectives and their interdependence as well as the sensitivity of the Pareto front to changes in the volume of component produced.

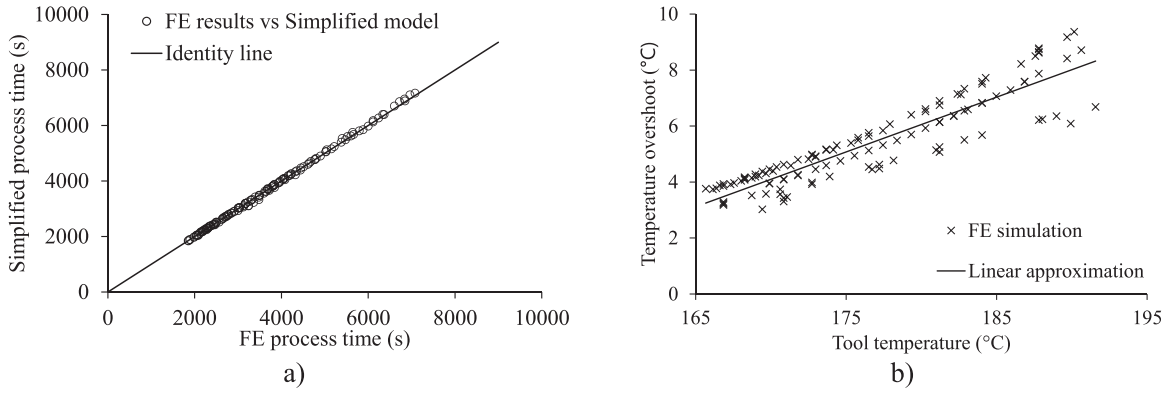

Fig. 13. Simplified approximation of 3D printing for the RTM6 epoxy/carbon fibre system: a) process duration; b) temperature overshoot.

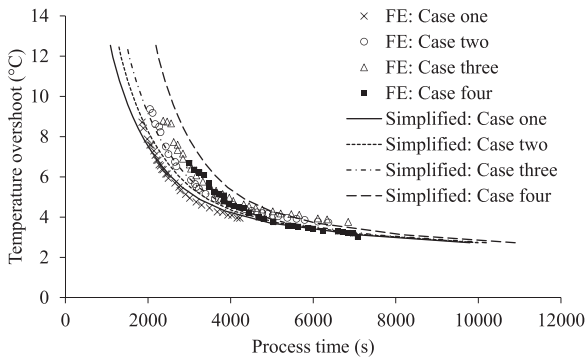

Fig. 14. Comparison of Pareto fronts obtained using FE simulation and the simplified model of 3D printing of the RTM6 epoxy/carbon fibre system.

The information captured by the simplified model can be used to explore the limits of the 3D printing process. Fig. 15a presents a process map of what can be achieved for different component sizes using the process parameters investigated in this work, i.e., maximum deposition speed of 600 mm/min, tow size of 2 mm × 2 mm and a single printing head. The process map presents the optimal Pareto fronts in terms of temperature overshoot and process time that can be achieved for increasing levels of components volumes. For low volume components, the efficient frontier of the process presents the L-shape observed previously with deposition and cure both contributing significantly to the total process duration. As the volume of the component increases, the Pareto front is dominated by the vertical region since the process duration is mainly governed by the deposition phase, with the cure having a small relative contribution. It should be noted that the extrapolation of simulation data implied by the simplified model of the process for large components necessitates an assumption of the process implementation being able to respect the constraint of limiting the curing of deposited layers before the next layer is processed to a degree of cure lower than gelation (0.59 for the resin system of this study). This can be accomplished by designing a heating system that follows the printing head to achieve local heating in the vicinity of deposition, with the rest of the component kept close to ambient temperature to avoid excessive curing.

Given that the 3D printing process limits the temperature overshoot to a few degrees, a point on the vertical part of the Pareto curves can be chosen to represent an efficient process. A selection of a moderate overshoot limit of 5 °C allows investigation of the influence of other parameters of the 3D printing process such as deposited tow width, maximum speed and number of printing heads used. Fig. 15b illustrates the dependence of process duration on component volume for different scenarios. The combination of tow width, printing speed and number of heads, for a given tow thickness of 2 mm used here, can be captured by the deposition rate calculated as the product of tow cross-sectional area, speed and number of printing heads. The range of deposition rates shown in Fig. 15b can be achieved with different combination of these parameters. For example, a deposition rate of 2 cm^3/min corresponds to a 2 mm wide tow deposited at 500 mm/min, whereas a rate of 32 cm^3/min can be achieved by using a speed of 1000 mm/min, four printing heads and a tow width of 4 mm. The dependence of process duration on volume is linear; the non-linearity shown in Fig. 15b is due to the log-log axes selected to facilitate visualisation across different orders of magnitude. The intercept in Fig. 15b is equal to the duration of the cure at the selected temperature, implied by the 5 °C temperature overshoot selected, and therefore it does not depend on the deposition rate of the printing process. Components with volumes below 10^3 cm^3 can be processed within a few hours. This range of volumes is typical of thin skins with a thickness of a few mm and areas below 1 m^2, and stiffeners or ribs with length in the order of 1 m and cross-sectional area in 1–10 cm^2 range. For components sizes in the order of 10^4 cm^3, typical of thick panels (thickness of 10–20 mm and area around 1 m^2) and integrated structures with thin skins and ribs, 3D printing can be completed within tens of hours. Large structures that reach 10^4 cm^3 in volume have processing times in the order of hundreds of hours and require use of multiple heads and wider tows to reduce the duration of printing to tens of hours. A multiple head system and local heating might be needed for complex geometries scenarios and large in-plane dimensions as a means for avoiding that the gelation point is exceeded. The durations reported here can be contrasted with the overall processing time involved in batch processing incorporating placement of reinforcement, debulking, consolidation and curing. For small components, the comparison only based on cure times is very favourable for 3D printing as reported in Section 4.2. Similarly for intermediate component sizes, taking into account that steps preceding curing usually have a similar duration to the cure, 3D printing represents a more efficient solution. For large components, the comparison is more complex as excessive tooling and heating apparatus costs need to be taken into account and contrasted with the cost of a multiple head printing system. Overall and once the ability of an additive process to process thicknesses not accessible through batch processing is taken into account, there is a clear case for the development of 3D printing of continuous fibre thermosetting composites as a means of increasing efficiency of composites manufacturing and expanding the use of lightweight materials into geometries currently not feasible through conventional means of processing.

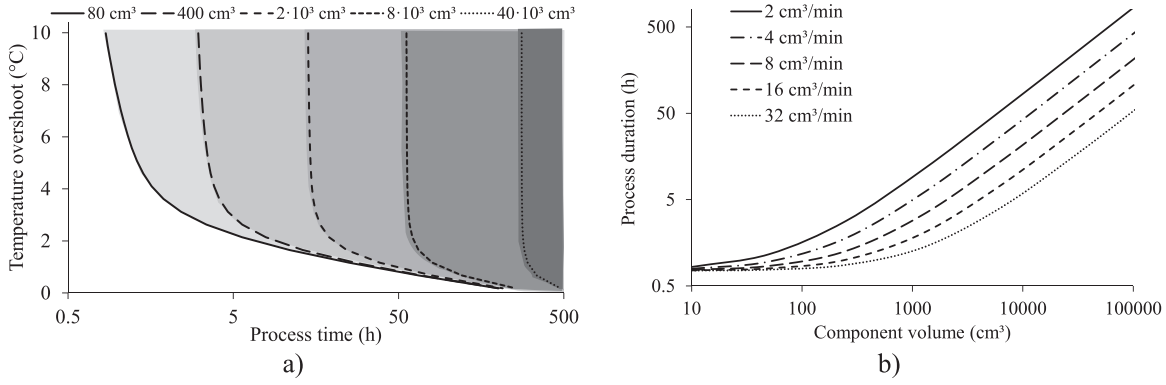

Fig. 15. Exploration of 3D printing process capabilities for the RTM6 epoxy/carbon fibre system: a) process map of Pareto fronts as a function of component volume for a maximum speed of 600 mm/min and a deposition tow size of 2 mm × 2 mm; b) 3D printing process duration as a function of component volume for different deposition rates (logarithmic scale).

4.4. Simplified analysis application to a prepreg system

The simplified methodology developed in Section 4.3 allows expanding the results to different epoxy resin systems. In this section, the HexPly® M21 prepreg epoxy system has been considered. Three FE based GA optimisation runs implementing HexPly® M21 material properties have been executed for Case I, II and III. The GA parameters and the ranges for the parameters are the same as those reported in Tables 4 and 5. The only difference compared to the formulation presented in Eq. (17) was that the constraint value for the degree of cure of the layer underlying the deposition ($\alpha_{underlying}$) was set to 0.51, based on the results for the gelation conversion of the M21 resin [24]. The optimisations were run for three generations achieving a satisfactory level of convergence. Following from the treatment for the Liquid Composite Moulding system in Eq. (21), a master curve describing the dependence on temperature overshoot on first dwell temperature was obtained for the results of the optimisation runs as follows:

$$\Delta T_{max} = 0.1773 T_1 - 29.57 \quad (22)$$

with temperatures expressed in °C. The process time from the simplified analysis can be calculated using Eq. 19 with a final degree of cure of 0.91, which the value calculated for the MRCC of the M21 system (180 °C for 2 h [24]) using the cure kinetics model reported in [35].

Fig. 16 presents a comparison of the three Pareto fronts from the full optimisation using FE cure simulation with the outcomes of the simplified analysis. The validated result for the MRCC conventional processing of a 24 mm thick component reported in [35] is also presented. A good agreement is found between the FE and simplified model Pareto fronts, confirming the validity of the simplified analysis. Furthermore, when the results are compared with the standard 24 mm thick laminate cure, it can be observed that the significant efficiency benefits of 3D printing reported for the LCM system in Section 4.2 are also manifested in the case of the prepreg system. More specifically, for a corner solution, there is a 60 % reduction in process time and 65 % in temperature overshoot.

Fig. 17 presents process maps obtained for the HexPly® M21 system based on the simplified analysis using Eqs. 20 and (22). Similar conclusions to the LCM system can be drawn for 3D printing of the prepreg. The 3D printing process results in a significant reduction of temperature overshoot, which makes processing of very thick components possible, even for configurations for which conventional processing is not feasible without violating constraints set on the maximum temperature reached. The process duration of 3D printing is significantly lower than conventional manufacturing for small components, with process completion within a few hours. Intermediate size components, with volumes of around 10^4 cm^3 require a few tens of hours or processing, a duration that is similar to current conventional manufacturing practices. Very large prepreg structures can be processed via 3D printing within realistic times with the utilisation of multiple heads and/or thick/wide tows. The maximum error in temperature overshoot estimation when the simplified model is used is of about 2 °C.

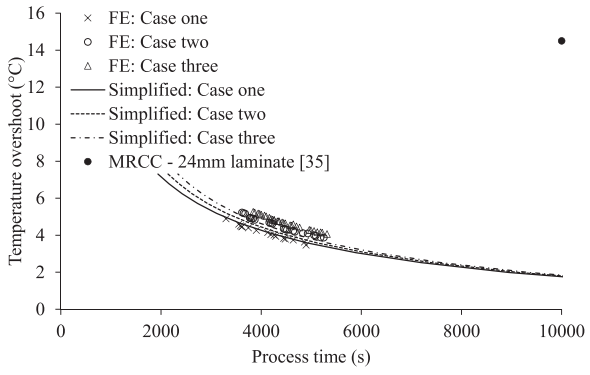

Fig. 16. Comparison of Pareto fronts obtained using FE simulation and the simplified model of 3D printing for the HexPly® M21 prepreg system.

5. Conclusions

In the pursuit of a first-time right design able to minimise material waste, defect generation and energy consumption for the composite manufacturing industry, 3D printing of continuous reinforced thermoset composite comes into play with the potential of meeting future targets especially in the manufacturing of thick and ultra-thick components, given its additive nature. The analysis reported in this paper underlines the significant benefits that 3D printing of continuous reinforced thermoset composite can bring to the composite manufacturing field. Application of optimisation to a 3D printing process and comparison with optimal batch processing conditions shows that improvements up to 50 % in process time and up to 85 % in temperature overshoot can be achieved when a 40 mm thick component with 800 mm^2 surface area is manufactured. Furthermore, the comparison among optimal solutions for different thicknesses (i.e. 20, 30 and 40 mm), shows that by manufacturing a component layer by layer, the strong non-linear dependence of temperature overshoot on thickness is eliminated. Consequently, components of greater thicknesses can be manufactured maintaining the same level of temperature overshoot. This reduces significantly the likelihood of unexpected detrimental defects in the final component (i.e. matrix cracking, residual stresses) which often cause part rejection and influence negatively the sustainability of the manufacturing process. The optimisation of a 150 mm long component (i.e. 30 cm^2 in plane dimension) demonstrated that manufacturing of larger components is possible with current printing speeds [41] with about 35 % process time reduction compared to conventional batch manufacturing. These outcomes are relevant to the unidirectional 3D printing case addressed here. Future extensions of this work to multi-angled laminates will address optimisation of deposition path and residual stress development to ensure the benefits established can be translated to generic components. Furthermore, the results of this study demonstrate the potential of the approach with respect to thermochemical phenomena only. Thermomechanical effects as well as influence of process parameters on mechanical performance will need to be elucidated in the future. The simplified analysis proposed predicts accurately the duration of the 3D printing process, allowing an efficient exploration of the process landscape. The validity of this analysis is a consequence of the linearisation of the process achieved through its additivity, which can be the basis for generic design and control methodologies in future implementations. According to this analysis, thin composite components with surface area of about 1 m^2 can be printed within few hours whilst thicker components in tens of hours. These process times compare favourably with conventional processes especially when all the manufacturing stages of conventional processes (lay-up, consolidation/infusion, curing and demoulding) are accounted for. These results are valid for state of art resins system in the aerospace sector processed using Liquid Composite Moulding or laying up-autoclaving. 3D printing adds to the traditional challenges several new process design degrees of freedom (i.e. degree of cure of deposited material before new material deposition, cooling effects of new deposited material, varying printing temperature degree of cure with thickness); which make the overall problem more complex and potentially not intuitive, but also providing additional flexibility. Based on the current findings, a pre-curing stage could be implemented to accelerate the curing process as depositing a partially cured filament with a degree of cure lower than gel conversion can further reduce exothermic reaction and process time without affecting mechanical properties. The pre-cured tow could also be manufactured separately and fed directly to the 3D printing head. Nevertheless, defects can be introduced upon deposition as the tow is deformed during printing, whilst the presence of voids and the consolidation state of the material are not controlled as directly as in the case of batch processing. Moreover, use of multiple

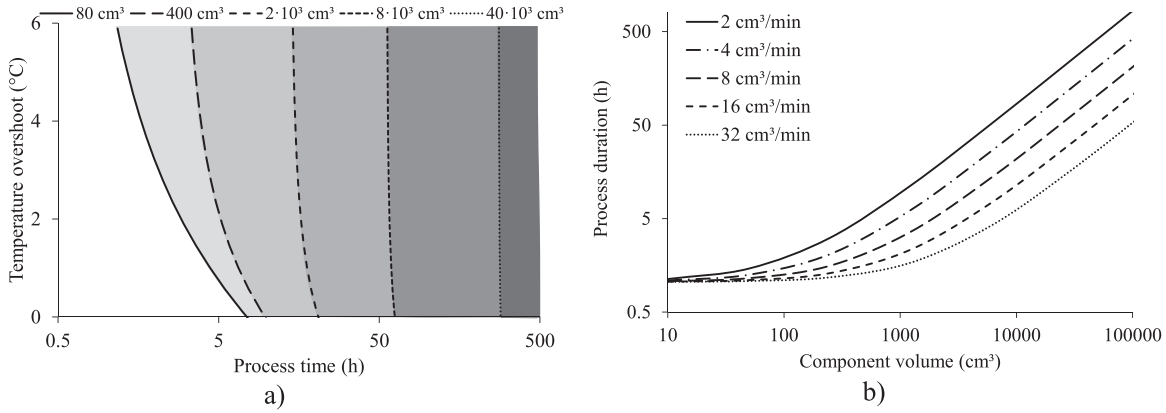

Fig. 17. Exploration of 3D printing process capabilities for the HexPly® M21 prepreg system: a) process map of Pareto fronts as a function of component volume for a maximum speed of 600 mm/min and a deposition tow size of 2 mm × 2 mm; b) 3D printing process duration as a function of component volume for different deposition rates (logarithmic scale).

deposition heads and wider tows is worth exploring to make 3D printing of large structures feasible within short processing times. Nevertheless, this development is expected to bring several technological challenges and additional overhead cost. Consolidation specifically represents a key development area to allow realising the predicted benefits; a consolidation roller after deposition or interruptions of the deposition process to allow intermediate consolidation steps using reusable bags, could be implemented. Thorough further investigation and technological development need to be carried out to overcome challenges and exploit the opportunities identified for 3D printing. Deposition induced defects such as gaps, overlaps, wrinkles and in-plane waviness can dramatically affect performance of the parts. These challenges need to be successfully overcome for the technology to achieve the potential shown in the current study. The results presented here show that the potential efficiency and capability benefits are significant and can transform the reach and impact of composites manufacturing.

CRediT authorship contribution statement

Giacomo Struzziero: Writing – original draft, Methodology, Investigation, Formal analysis, Data curation, Conceptualization. **Michel Barbezat:** Writing – review & editing. **Alexandros A. Skordos:** Writing – review & editing, Conceptualization.

Declaration of Competing Interest

The authors declare that they have no known competing financial interests or personal relationships that could have appeared to influence the work reported in this paper.

Data Availability

Research data can be found at https://doi.org/10.5281/zenodo.7540338.

Acknowledgements

This work was supported by the Laboratory for Mechanical Systems Engineering, Swiss Federal Laboratories for Materials Science and Technology (Empa) through the Empa board of directors (project code AP304-2124) and by the Engineering and Physical Sciences Research Council [grant number EP/P006701/1]; through the EPSRC Future Composites Manufacturing Research Hub. The authors would like to acknowledge Dr Mesogitis for helpful discussions regarding the HexPly M21 prepreg system material models. The authors are grateful to Wenchang Zhang, Northwestern Polytechnical University, for identifying an error in the analysis contained in the original version of this paper.

References

[1] G. Struzziero, J.J.E. Teuwen, A.A. Skordos, Numerical optimisation of thermoset composites manufacturing processes: a review, Compos. Part A: Appl. Sci. Manuf. 124 (2019), 105499.
[2] M. Li, Q. Zhu, P.H. Geubelle, C.L. Tucker III, Optimal curing for thermoset matrix composites: Thermochemical considerations, Polym. Compos. 22 (1) (2001) 118–131.
[3] N. Rai, R. Pitchumani, Optimal cure cycles for the fabrication of thermosetting-matrix composites, Polym. Compos. 18 (4) (1997) 566–581.
[4] Z.L. Yang, Optimized curing of thick section composite laminates, Mater. Manuf. Process. 16 (4) (2001) 541–560.
[5] J.L. Bailleul, V. Sobotka, D. Delaunay, Y. Jarny, Inverse algorithm for optimal processing of composite materials, Compos. Part A: Appl. Sci. Manuf. 34 (8) (2003) 695–708.
[6] S.R. White, H.T. Hahn, Cure cycle optimization for the reduction of processing-induced residual stresses in composite materials, J. Compos. Mater. 27 (14) (1993) 1352–1378.
[7] R. Matsuzaki, R. Yokoyama, T. Kobara, T. Tachikawa, Multi-objective curing optimization of carbon fiber composite materials using data assimilation and localized heating, Compos. Part A: Appl. Sci. Manuf. 119 (2019) 61–72.
[8] G. Struzziero, J.J.E. Teuwen, Effect of convection coefficient and thickness on optimal cure cycles for the manufacturing of wind turbine components using VARTM, Compos. Part A: Appl. Sci. Manuf. 123 (2019) 25–36.
[9] M. Araya-Calvo, I. López-Gómez, N. Chamberlain-Simon, J.L. León-Salazar, T. Guillén-Girón, J.S. Corrales-Cordero, et al., Evaluation of compressive and flexural properties of continuous fiber fabrication additive manufacturing technology, Addit. Manuf. 22 (2018) 157–164.
[10] A.N. Dickson, J.N. Barry, K.A. McDonnell, D.P. Dowling, Fabrication of continuous carbon, glass and Kevlar fibre reinforced polymer composites using additive manufacturing, Addit. Manuf. 16 (2017) 146–152.
[11] M. Eichenhofer, J.C.H. Wong, P. Ermanni, Continuous lattice fabrication of ultra-lightweight composite structures, Addit. Manuf. 18 (2017) 48–57.
[12] H.J. O'Connor, D.P. Dowling, Evaluation of the influence of low pressure additive manufacturing processing conditions on printed polymer parts, Addit. Manuf. 21 (2018) 404–412.
[13] P. Parandoush, C. Zhou, D. Lin, 3D printing of ultrahigh strength continuous carbon fiber composites, Adv. Eng. Mater. 21 (2) (2019) 1800622.
[14] W. Hao, Y. Liu, H. Zhou, H. Chen, D. Fang, Preparation and characterization of 3D printed continuous carbon fiber reinforced thermosetting composites, Polym. Test. 65 (2018) 29–34.
[15] Y. Ming, Z. Xin, J. Zhang, Y. Duan, B. Wang, Fabrication of continuous glass fiber-reinforced dual-cure epoxy composites via UV-assisted fused deposition modeling, Compos. Commun. 21 (2020), 100401.
[16] Y. Ming, S. Zhang, W. Han, B. Wang, Y. Duan, H. Xiao, Investigation on process parameters of 3D printed continuous carbon fiber-reinforced thermosetting epoxy composites, Addit. Manuf. 33 (2020), 101184.
[17] H. Xiao, W. Han, Y. Ming, Z. Ding, Y. Duan, A sensitivity analysis-based parameter optimization framework for 3d printing of continuous carbon fiber/epoxy composites, Materials 12 (23) (2019) 3961.
[18] Y. Ming, Y. Duan, B. Wang, H. Xiao, X. Zhang, A novel route to fabricate high-performance 3d printed continuous fiber-reinforced thermosetting polymer composites, Materials 12 (9) (2019) 1369.
[19] Skordos A.A., Kratz J. Layer by Layer (LbL) curing - Feasibility study. ⟨https://cimcomp.ac.uk/wp-content/uploads/2017/11/Executive-Summary.pdf⟩.

[20] G. Struzziero, J.J.E. Teuwen, A fully coupled thermo-mechanical analysis for the minimisation of spring-in and process time in ultra-thick components for wind turbine blades, Compos. Part A: Appl. Sci. Manuf. 139 (2020), 106105.
[21] Dassault Systemes Abaqus® Documentation, 2019.
[22] Hexcel. HexForce® G1157 D1300, ⟨www.hexcel.com⟩.
[23] Hexcel® RTM 6 epoxy system for Resin Transfer Moulding monocomponent system product data. ⟨www.hexcel.com⟩.
[24] HexPly® M21 180 °C (350 °F) curing epxy matrix product data. ⟨www.hexcel.com⟩.
[25] N. Rai, R. Pitchumani, Rapid cure simulation using artificial neural networks, Compos. Part A: Appl. Sci. Manuf. 28 (9) (1997) 847–859.
[26] V. Antonucci, M. Giordano, S. Inserraimparato, L. Nicolais, Analysis of heat transfer in autoclave technology, Polym. Compos. 22 (5) (2001) 613–620.
[27] A.B. Etemoglu, M.K. Isman, M. Can, Investigation into the effect of nozzle shape on the nozzle discharge coefficient and heat and mass transfer characteristics of impinging air jets, Heat Mass Transf. 46 (11) (2010) 1395–1410.
[28] V. Katti, S.V. Prabhu, Experimental study and theoretical analysis of local heat transfer distribution between smooth flat surface and impinging air jet from a circular straight pipe nozzle, Int. J. Heat. Mass Transf. 51 (17) (2008) 4480–4495.
[29] D. Lytle, B.W. Webb, Air jet impingement heat transfer at low nozzle-plate spacings, Int. J. Heat Mass Transf. 37 (12) (1994) 1687–1697.
[30] M. Nirmalkumar, V. Katti, S.V. Prabhu, Local heat transfer distribution on a smooth flat plate impinged by a slot jet, Int. J. Heat Mass Transf. 54 (1) (2011) 727–738.
[31] G. Struzziero, A.A. Skordos, Multi-objective optimisation of the cure of thick components, Compos. Part A: Appl. Sci. Manuf. 93 (2017) 126–136.
[32] P.I. Karkanas, I.K. Partridge, Cure modeling and monitoring of epoxy/amine resin systems. I. Cure kinetics modeling, J. Appl. Polym. Sci. 77 (7) (2000) 1419–1431.
[33] P.I. Karkanas, I.K. Partridge, D. Attwood, Modelling the cure of a commercial epoxy resin for applications in resin transfer moulding, Polym. Int. 41 (2) (1996) 183–191.
[34] A.A. Skordos, I.K. Partridge, Inverse heat transfer for optimization and on-line thermal properties estimation in composites curing, Inverse Probl. Sci. Eng. 12 (2) (2004) 157–172.
[35] T. Mesogitis, J. Kratz, A.A. Skordos, Heat transfer simulation of the cure of thermoplastic particle interleaf carbon fibre epoxy prepregs, J. Compos. Mater. 53 (15) (2019) 2053–2064.
[36] J.P. Pascault, R.J.J. Williams, Glass transition temperature versus conversion relationships for thermosetting polymers, J. Polym. Sci. Part B: Polym. Phys. 28 (1) (1990) 85–95.
[37] G. Struzziero, A.A. Skordos, Multi-objective optimization of Resin Infusion, Adv. Manuf.: Polym. Compos. Sci. 5 (1) (2019) 17–28.
[38] J.D. Farmer, E.E. Covert, Thermal conductivity of a thermosetting advanced composite during its cure, J. Thermophys. Heat. Transf. 10 (3) (1996) 467–475.
[39] C. Formicola, A. De Fenzo, M. Zarrelli, A. Frache, M. Giordano, G. Camino, Synergistic effects of zinc borate and aluminium trihydroxide on flammability behaviour of aerospace epoxy system, EXPRESS Polym. Lett. 3 (6) (2009) 376–384.
[40] P.I. Karkanas, I.K. Partridge, Cure modeling and monitoring of epoxy/amine resin systems. II. Network formation and chemoviscosity modeling, J. Appl. Polym. Sci. 77 (10) (2000) 2178–2188.
[41] G. Struzziero, M. Barbezat, A.A. Skordos, Consolidation of continuous fibre reinforced composites in additive processes: a review, Addit. Manuf. (2021), 102458.